Nanomaterials

International Edition: DOI: 10.1002/anie.201814492
German Edition: DOI: 10.1002/ange.201814492

Spatially Controlled Occlusion of Polymer-Stabilized Gold Nanoparticles within ZnO

Yin Ning, Lee A. Fielding, John Nutter, Alexander N. Kulak, Fiona C. Meldrum, and Steven P. Armes**

Abstract: *In principle, incorporating nanoparticles into growing crystals offers an attractive and highly convenient route for the production of a wide range of novel nanocomposites. Herein we describe an efficient aqueous route that enables the spatially controlled occlusion of gold nanoparticles (AuNPs) within ZnO crystals at up to 20% by mass. Depending on the precise synthesis protocol, these AuNPs can be (i) solely located within a central region, (ii) uniformly distributed throughout the ZnO host crystal or (iii) confined to a surface layer. Remarkably, such efficient occlusion is mediated by a non-ionic water-soluble polymer, poly(glycerol monomethacrylate)$_{70}$ (G_{70}), which is chemically grafted to the AuNPs; pendent cis-diol side groups on this steric stabilizer bind Zn^{2+} cations, which promotes nanoparticle interaction with the growing ZnO crystals. Finally, uniform occlusion of G_{70}-AuNPs within this inorganic host leads to faster UV-induced photodegradation of a model dye.*

Natural biominerals, such as bones, teeth, and seashells, provide many wonderful examples of the incorporation of water-soluble biomacromolecules within various inorganic crystals.[1] However, incorporating nanoparticles into inorganic crystals is much more challenging.[2] This is partly because crystallization normally favours impurity expulsion, rather than occlusion.[3] Nevertheless, various inorganic nanoparticles (e.g. Pt, Au, Fe_3O_4, quantum dots, etc.) have been encapsulated into zeolites,[4] metal–organic frameworks (MOFs),[5] and ionic crystals,[6] albeit typically at relatively low loadings. In related work, inorganic nanoparticles can also be incorporated into $CaCO_3$ (calcite)[7] and Cu_2O[8] using either a gel-trapping or a confinement-based strategy, respectively.

There is a growing number of literature reports describing the occlusion of various anionic nanoparticles with appropriate surface functionality (such as carboxylate,[9] sulfonate,[10] and sulfate groups[11]) within single crystals (e.g. calcite or ZnO). Such wholly synthetic systems provide a new approach for the preparation of new nanocomposite crystals, while enabling the convenient introduction of color,[7a,b] magnetism,[7b] fluorescence,[6] or enhanced mechanical properties (e.g. hardness).[9b] However, good control over the spatial distribution of guest nanoparticles within growing host inorganic crystals has not yet been achieved.

Herein we report the efficient, spatially controlled occlusion of non-ionic poly(glycerol monomethacrylate)$_{70}$-stabilized gold nanoparticles (G_{70}-AuNPs; see the Supporting Information for further synthesis and characterization details, Figures S1–S4) within ZnO crystals generated in aqueous solution (Scheme 1). It is emphasized that this occlusion strategy differentiates our work from the many literature examples of Au/ZnO nanocomposites in which AuNPs are merely adsorbed at the surface of ZnO crystals.[12] Serendipitously, we found that G_{70}-AuNPs were efficiently incorporated within ZnO crystals generated by heating an aqueous solution containing $Zn(NO_3)_2{\cdot}6H_2O$ and hexamethylenetetramine at 90 °C for 1.5 h. In the absence of any G_{70}-AuNPs, twinned ZnO rods were obtained (Figure 1a). In the presence of 0.01 g dm^{-3} G_{70}-AuNPs (Au core diameter = 4.8 nm), nanoparticle occlusion was mainly confined to the central region of the ZnO rods, as indicated by the bracket shown in Figure 1b. [In addition, larger G_{70}-AuNPs (Au core diameter = 14 nm) were also prepared to aid nanoparticle imaging within the central region of the ZnO rods via SEM, see Figure S5]. Using a higher concentration of 4.8 nm G_{70}-AuNPs (0.05 g dm^{-3}) led to a larger central zone (Figure 1c, see brackets). When a concentration of 0.075 g dm^{-3} was utilized, essentially all the G_{70}-AuNPs are more or less uniformly distributed throughout the ZnO crystals (Figure S6). At 0.10 g dm^{-3}, the G_{70}-AuNPs are uniformly occluded within the ZnO crystals (Figure 1d). The selected-area electron diffraction (SAED) pattern obtained for the ZnO control prepared in the absence of any nanoparticles (see inset in Figure 1a) confirmed its single-crystal nature. The same SAED pattern plus an additional ring of diffraction spots corresponding to AuNPs was observed for the G_{70}-Au(uniform)/ZnO nanocomposite crystals (see right inset in Figure 1d). Powder XRD studies confirmed that the ZnO particles always exhibited the wurtzite structure, whether they

[*] Dr. Y. Ning, Prof. S. P. Armes
Department of Chemistry, University of Sheffield
Brook Hill, Sheffield, South Yorkshire S3 7HF (UK)
E-mail: Y.Ning@sheffield.ac.uk
s.p.armes@sheffield.ac.uk
Dr. L. A. Fielding
The School of Materials, University of Manchester
Oxford Road, Manchester M13 9PL (UK)
J. Nutter
Henry Royce Institute
Department of Materials Science and Engineering
University of Sheffield
Mappin Street, Sheffield S1 3JD (UK)
Dr. A. N. Kulak, Prof. F. C. Meldrum
School of Chemistry, University of Leeds
Woodhouse Lane, Leeds LS2 9JT (UK)
Supporting information and the ORCID identification numbers for some of the authors of this article can be found under: https://doi.org/10.1002/anie.201814492.

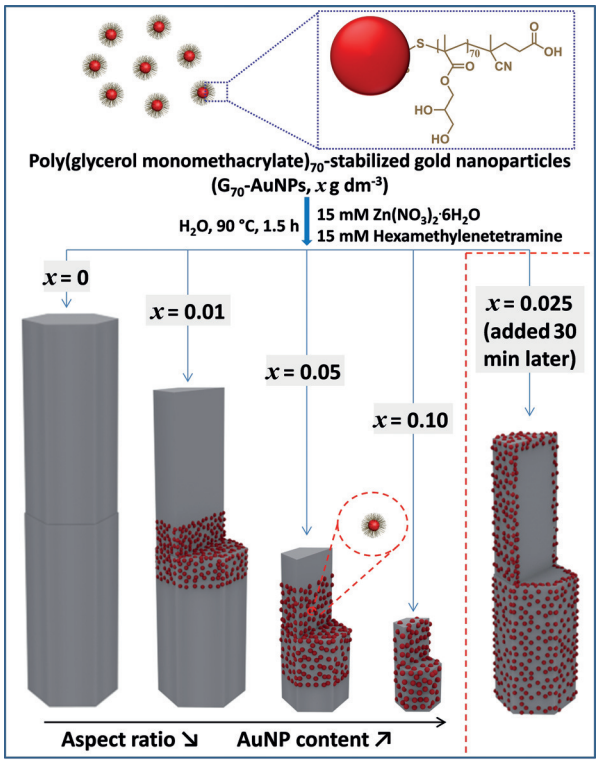

Scheme 1. Schematic representation of spatially controlled occlusion of non-ionic poly(glycerol monomethacrylate)$_{70}$-stabilized gold nanoparticles (G_{70}-AuNPs) within ZnO crystals. A twinned hexagonal rod-like ZnO crystal is obtained in the absence of any G_{70}-AuNPs ($x=0$). In the presence of G_{70}-AuNPs, shorter twinned hexagonal ZnO rods are obtained. For $x=0.01$ and 0.05, the G_{70}-AuNPs are preferentially located within the central region of the rods. In contrast, uniform spatial occlusion is achieved for $x=0.10$. Finally, if the G_{70}-AuNP addition is delayed for 30 min when $x=0.025$ is used, then only surface-confined occlusion is observed.

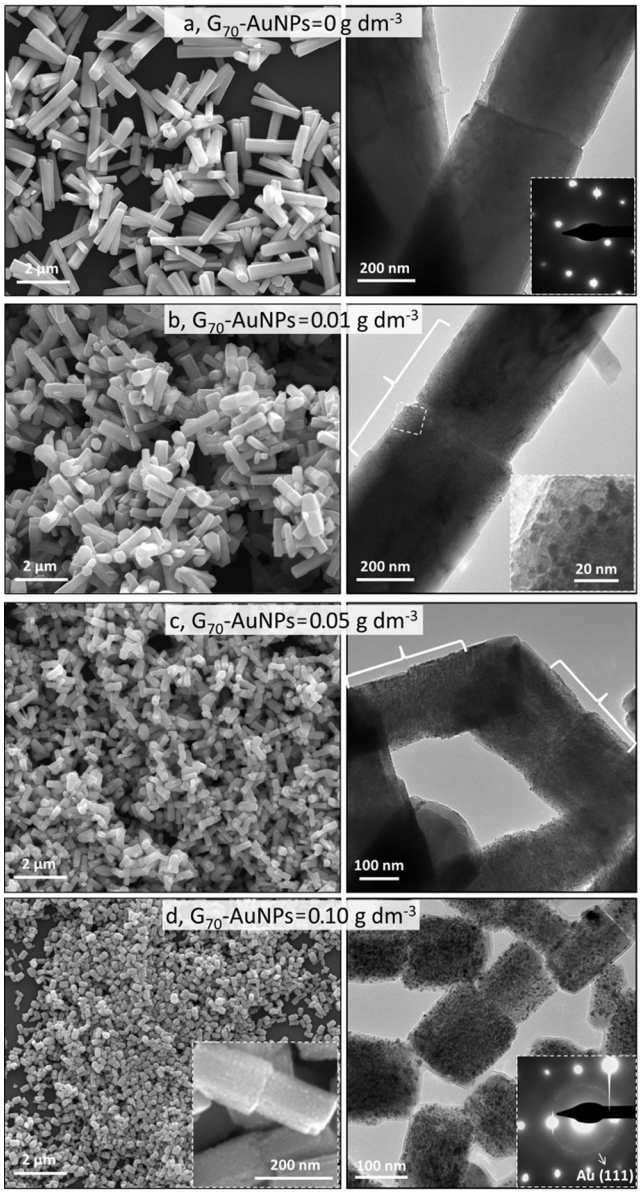

Figure 1. SEM images (left column) and TEM images (right column) obtained for ZnO crystals prepared in the presence of various concentrations (x) of G_{70}-AuNPs. a) $x=0$ g dm^{-3} (pure ZnO control); b) $x=0.01$ g dm^{-3}; c) $x=0.05$ g dm^{-3}; d) $x=0.10$ g dm^{-3}. The insets in (a) and (d) in the TEM images represent selected-area electron diffraction (SAED) patterns recorded for the corresponding sample. The inset shown in (b) is a higher magnification TEM image of the indicated region. The left inset in (d) is a higher magnification SEM image showing ZnO rods surface-decorated with gold nanoparticles (see white dots). The SAED pattern in the right inset in (d) indicates the single-crystal nature of these ZnO particles and also a ring of diffraction spots assigned to the Au (111) planes. The white brackets in (b) and (c) show the spatial location of the AuNPs within the central region of the ZnO rods.

were prepared in the presence or absence of G_{70}-AuNPs (Figure S7).

High-resolution TEM images recorded for ultramicrotomed G_{70}-Au/ZnO nanocomposite crystals embedded in epoxy resin confirmed that the G_{70}-AuNPs were incorporated within the host matrix, rather than merely being deposited on its surface (Figure 2). When the cross-section parallel to the c axis of the ZnO crystals was imaged (Figures 2a–d), G_{70}-AuNPs (which appear darker than the host crystal owing to their higher electron density) are clearly preferentially located within the central core of the ZnO rods when G_{70}-AuNPs were used at a relatively low concentration of 0.05 g dm^{-3} (denoted as G_{70}-Au(central)/ZnO, Figures 2a–c). In contrast, a uniform distribution of AuNPs throughout the ZnO crystal was achieved at 0.10 g dm^{-3} (denoted as G_{70}-Au(uniform)/ZnO, Figure 2d). The spatial distribution of AuNPs was further examined by imaging cross-sections made perpendicular to the c axis of the G_{70}-Au/ZnO rods (Figures 2e–n). In a control experiment, ultramicrotomed ZnO crystals prepared in the absence of any AuNPs exhibited the expected hexagonal shape (Figure 2e).[13] When 0.10 g dm^{-3} G_{70}-AuNPs was used, G_{70}-AuNPs were homogeneously occluded throughout the ZnO rods (Figure 2f). At this point, we hypothesized that ZnO crystals might also be prepared in which G_{70}-AuNPs are solely located within a surface layer. This objective was achieved via delayed addition of the G_{70}-AuNPs during ZnO formation. Under such conditions, ultramicrotomed cross-sections confirmed

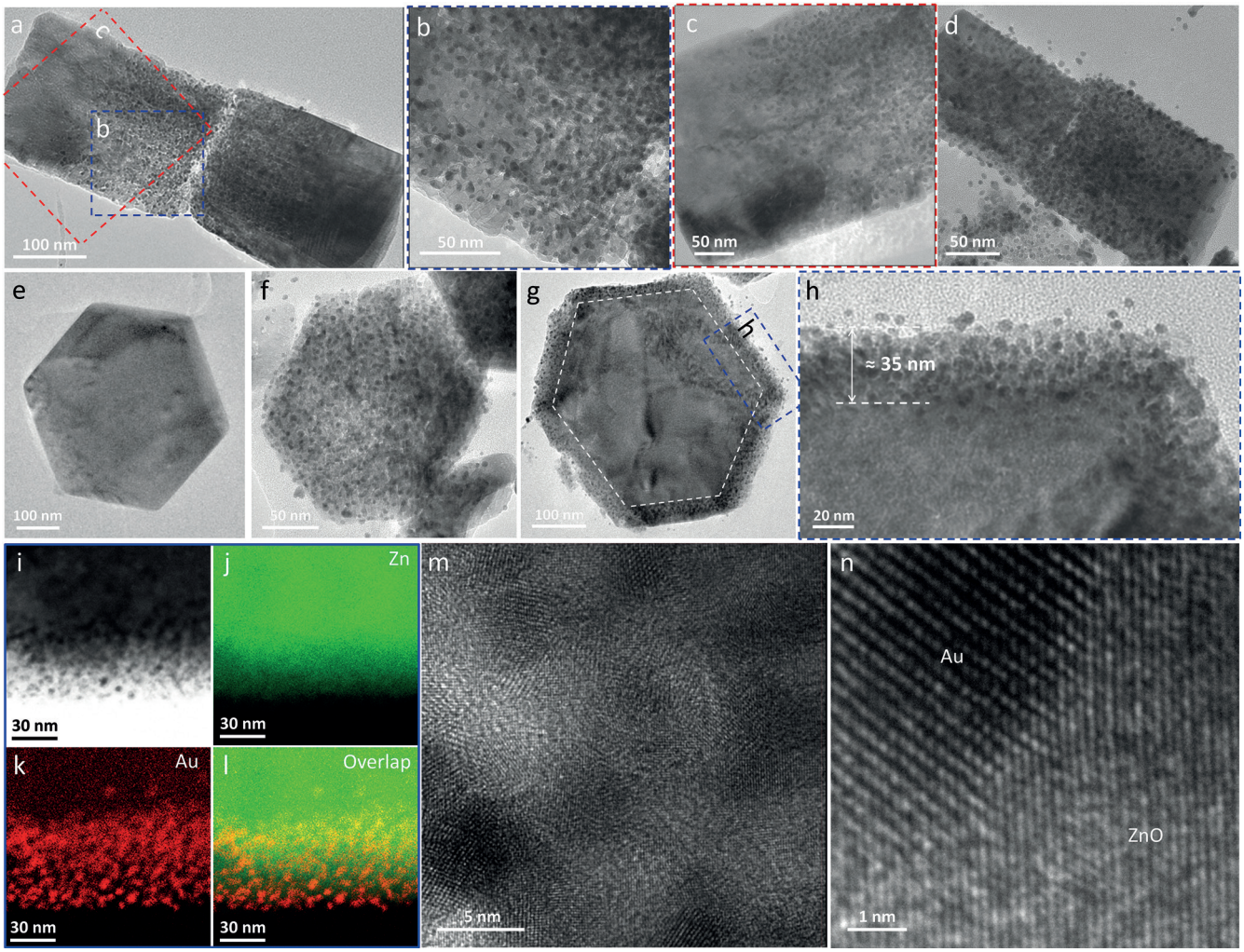

Figure 2. TEM images of ultramicrotomed cross-sections of G_{70}-Au/ZnO nanocomposite crystals that are a)–d) parallel to the *c* axis and e)–n) perpendicular to the *c* axis. a–c) 0.05 g dm^{-3} G_{70}-Au(central)/ZnO, with (b) and (c) representing magnified regions, as indicated in (a); d) 0.10 g dm^{-3} G_{70}-Au(uniform)/ZnO; e) ZnO control; f) 0.10 g dm^{-3} G_{70}-Au(uniform)/ZnO; g, h) G_{70}-Au(surface)/ZnO with G_{70}-AuNPs occluded within ZnO rod-like crystals in the form of a ≈35 nm surface layer; i)–l) STEM-EDS elemental mapping of Zn and Au for G_{70}-Au(surface)/ZnO. m) High-resolution TEM images of uniformly distributed AuNPs within ZnO and n) the interface between the AuNPs and the ZnO host. The black dots in (m) indicate the AuNPs while in (n) it is clear that there is no amorphous ZnO or polymer layer at the interface between an individual AuNP and the ZnO lattice.

that G_{70}-AuNPs are mainly confined to a ≈35 nm surface layer within the ZnO crystal (denoted as G_{70}-Au(surface)/ZnO), as shown in Figure 2g,h. STEM-EDS elemental mapping for Zn and Au further confirms the surface-confined occlusion of AuNPs within the host ZnO crystals (see Figure 2i–l).

Figure 2m,n shows high-resolution TEM images obtained for the G_{70}-Au(uniform)/ZnO sample, in which lattice fringes of Au and ZnO can be clearly observed. Importantly, no interfacial amorphous ZnO (or G_{70} layer) between the guest AuNP and host ZnO was observed (see Figure 2n). Further high-magnification TEM images are shown in Figures S8 and S9. Given the presence of the G_{70} stabilizer chains at the surface of the AuNPs, it is perhaps surprising that no distinct interfacial region is observed between the AuNPs and the ZnO matrix (Figure 2n). However, the surface density of the G_{70} chains on the AuNPs is calculated (see the Supporting Information) to be approximately 0.54 chains nm^{-2}, which is relatively low.[14] Hence ZnO crystal growth can penetrate within the G_{70} stabilizer layer, leading to intimate contact with the AuNP cores. This was confirmed by XPS studies, which indicate a charge transfer interaction between Au and ZnO (Figure S10). In this context, it is perhaps noteworthy that Asenath-Smith et al.[8b] also reported intimate contact between guest citrate-stabilized AuNPs and host Cu_2O crystals. Furthermore, Kulak et al.[10] did not observe any interfacial host–guest region for block copolymer-stabilized magnetite sols occluded within either calcite or ZnO.

The extent of G_{70}-AuNPs occlusion within ZnO increased when higher G_{70}-AuNP concentrations were used, as determined by inductively coupled plasma mass spectrometry (ICP-MS, Table S1). Remarkably, ZnO crystals containing up to 11.9% gold by mass (or 19.9% G_{70}-AuNPs by mass) can be prepared under uniform occlusion conditions (for example, when 0.10 g dm^{-3} G_{70}-AuNPs is used). Clearly, the G_{70} stabilizer chains play a key role in the interaction between

the AuNPs and the growing host crystal. At first sight this seems rather counterintuitive because the non-ionic nature of the poly(glycerol monomethacrylate) stabilizer chains might be expected to produce little or no interaction with the ZnO lattice. Indeed, previous reports suggest that anionic surface charge density is required for efficient interaction of copolymer nanoparticles within calcite or ZnO crystals.[9–11] The G_{70} chains used in this study contain a terminal carboxylic acid unit but further experiments confirmed that such anionic end-groups are not actually required to achieve efficient occlusion within ZnO (Figure S11). So how do the G_{70}-AuNPs interact with the growing ZnO? Bearing in mind a report by Cölfen and co-workers on polyacrylamide interactions with ZnO crystals,[15] the most likely explanation involves chelation between the Zn^{2+} cations and the *cis*-diol groups on the non-ionic G_{70} stabilizer chains.[16] Experimental evidence for this complexation is provided by vibrational spectroscopy (Figure 3a). In FTIR spectra recorded for G_{70}-AuNPs and G_{70} homopolymer, the absorption bands at 1255 cm^{-1} and 1275 cm^{-1} are assigned to the in-plane bending vibrations of primary and secondary C–OH, respectively.[17] These two bands merge to form a single new band at 1264 cm^{-1} for G_{70}-Au/ZnO nanocomposites, which supports the postulated chelation of Zn^{2+} cations by the G_{70} chains (see inset shown in Figure 3a and also Figure S12 for the control experiment conducted in the presence of a stoichiometric amount of $Zn(NO_3)_2$).[18]

Compared to the ZnO control, the mean length and width of the G_{70}-Au/ZnO nanocomposite crystals are systematically reduced when they are grown in the presence of higher concentrations of G_{70}-AuNPs (Figure 3b). More specifically, the mean length is dramatically reduced relative to the mean width, resulting in a much lower aspect ratio for the anisotropic ZnO crystals. This reduction in size cannot be avoided and indicates that G_{70}-AuNPs bind preferentially to the polar (0001) face relative to the six non-polar (100) faces, thereby retarding the crystal growth rate and producing less anisotropic ZnO rods (see the Supporting Information for more detailed discussion).[9a] Preparation of "core–shell" G_{70}-Au/ZnO crystals was also attempted but only G_{70}-Au(central)/ZnO structures were obtained. This is presumably because the ZnO precursor cannot grow effectively on (100) faces after delayed addition but instead grows preferentially on the (0001) face (see Scheme S1). At a relatively low G_{70}-AuNP concentration (i.e. below 0.05 g dm^{-3}), nanoparticle occlusion is complete before ZnO crystallization has ceased, leading to G_{70}-AuNPs being confined within a central region. At higher G_{70}-AuNP concentrations, there are sufficient G_{70}-AuNPs present to become occluded throughout the host crystal, while ZnO growth is significantly retarded.

Finally, we briefly explored the photocatalytic properties of these Au/ZnO nanocomposite crystals with different spatial distributions of AuNPs. Preliminary data confirm that the rate of UV photodegradation of a model rhodamine B dye increases monotonically with their AuNP content (Figure 3c). More importantly, the catalytic efficiency obtained for G_{70}-Au(uniform)/ZnO significantly exceeds that of G_{70}-Au(surface)/ZnO, which suggests that uniform occlusion of G_{70}-AuNPs within ZnO promotes catalytic performance (see control experiments in Figure S13 and further discussion in the Supporting Information). This suggests that a higher extent of AuNP occlusion within ZnO may provide a larger number of electron "sinks". If this is correct, it should facilitate charge carrier separation and extend the lifetime of

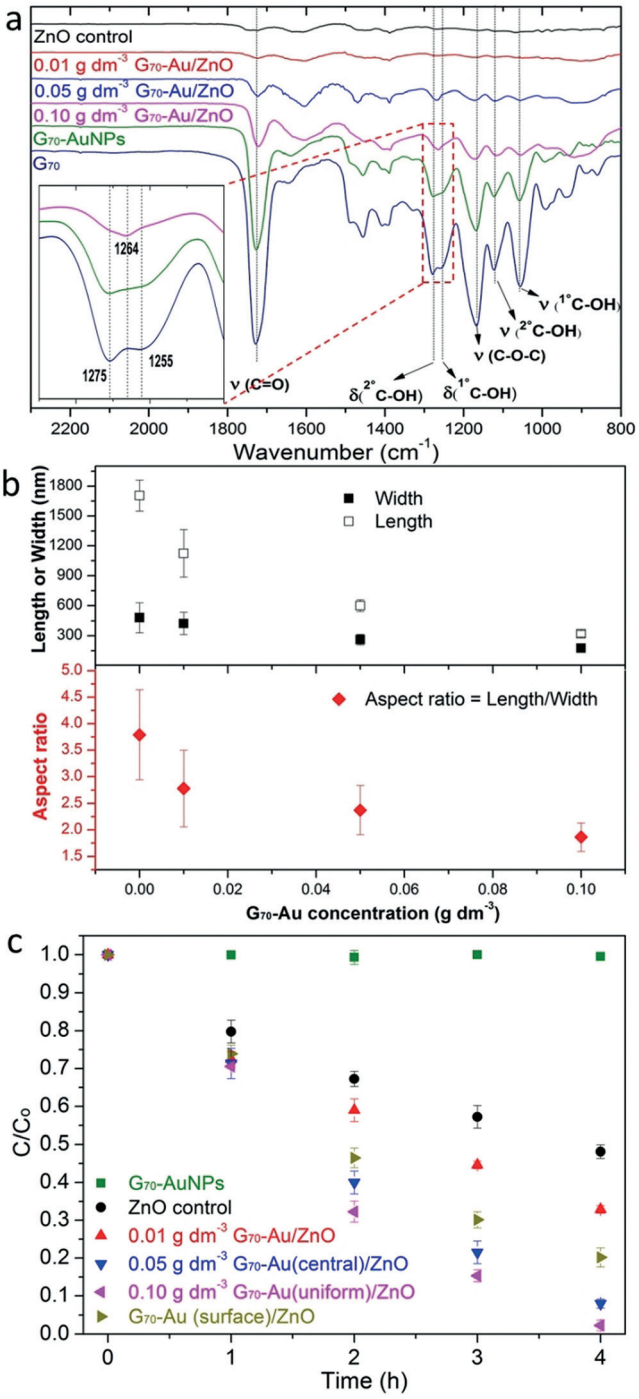

Figure 3. a) FTIR spectra recorded for three G_{70}-Au/ZnO nanocomposite crystals and three reference materials (ZnO crystals alone, G_{70} homopolymer, and G_{70}-AuNPs). b) Length, width, and aspect ratio of G_{70}-Au/ZnO versus G_{70}-AuNP concentration; c) UV photocatalytic decomposition rates observed at 20°C and pH 7 (6 W source, $\lambda = 254$ nm) for a model rhodamine B dye in the presence of four G_{70}-Au/ZnO nanocomposite crystals and two control samples.

the electron–hole pair,[12a,b,19] thus producing a more effective photocatalyst.

In summary, we report an efficient, versatile, and scalable route to incorporate sterically stabilized gold nanoparticles within ZnO single crystals. This study provides the first example of nanoparticle occlusion within inorganic crystals with well-controlled spatial distribution as well as tunable extent of occlusion, which offers an unprecedented opportunity to elucidate synthesis–structure–property relationships. We show for the first time that a non-ionic polymer stabilizer can promote highly efficient nanoparticle occlusion into inorganic host crystals. This represents an important paradigm shift because almost all prior literature reports in this field utilize anionic polymers as steric stabilizers. We rationalize the occlusion mechanism in terms of Zn^{2+} complexation to the non-ionic stabilizer chains and demonstrate that incorporation of AuNPs into ZnO crystals enhances their photocatalytic performance. In principle, appropriate surface modification of various other metal nanoparticles should enable their efficient occlusion within ZnO (and perhaps other host crystals), thus providing access to a range of new functional nanocomposite materials that are likely to exhibit emergent properties. We intend to explore this concept in the near future.

Acknowledgements

The Overseas Study Program of Guangzhou Elite Project and EPSRC (EP/P005241/1) are acknowledged for PhD sponsorship and post-doctoral support of Y.N., respectively. We thank EPSRC for post-doctoral support (EP/J018589/1 and EP/K006290/1) and S.P.A. also acknowledges a five-year ERC Advanced Investigator grant (PISA 320372). We thank Prof. G. J. Leggett and Dr. D. Hammond for useful XPS discussion, Prof. B. Inkson and Dr. S. Tzokov for TEM assistance, and Dr. C. Hill for ultramicrotomy. We also thank the University of Sheffield Sorby Centre for HRTEM access.

Conflict of interest

The authors declare no conflict of interest.

Keywords: gold nanoparticles · nanocomposites · nanomaterials · RAFT polymerization · ZnO

How to cite: *Angew. Chem. Int. Ed.* **2019**, *58*, 4302–4307
Angew. Chem. **2019**, *131*, 4346–4351

[1] a) A. Berman, L. Addadi, S. Weiner, *Nature* **1988**, *331*, 546–548; b) A. Berman, L. Addadi, A. Kvick, L. Leiserowitz, M. Nelson, S. Weiner, *Science* **1990**, *250*, 664–667; c) H. A. Lowenstam, S. Weiner, *On Biomineralization*, Oxford University Press, New York, **1989**; d) S. Mann, D. D. Archibald, J. M. Didymus, T. Douglas, B. R. Heywood, F. C. Meldrum, N. J. Reeves, *Science* **1993**, *261*, 1286–1292; e) A. M. Belcher, X. H. Wu, R. J. Christensen, P. K. Hansma, G. D. Stucky, D. E. Morse, *Nature* **1996**, *381*, 56–58; f) S. Mann, *Biomineralization: principles and concepts in bioinorganic materials chemistry*, Oxford University Press, Oxford, **2001**; g) A.-W. Xu, Y. Ma, H. Cölfen, *J. Mater. Chem.* **2007**, *17*, 415–449; h) F. C. Meldrum, H. Cölfen, *Chem. Rev.* **2008**, *108*, 4332–4432; i) E. Weber, B. Pokroy, *CrystEngComm* **2015**, *17*, 5873–5883; j) F. Nudelman, N. A. Sommerdijk, *Angew. Chem. Int. Ed.* **2012**, *51*, 6582–6596; *Angew. Chem.* **2012**, *124*, 6686–6700.

[2] a) J. D. Pasteris, J. J. Freeman, B. Wopenka, K. Qi, Q. Ma, K. L. Wooley, *Astrobiology* **2006**, *6*, 625–643; b) C. H. Lu, L. M. Qi, H. L. Cong, X. Y. Wang, J. H. Yang, L. L. Yang, D. Y. Zhang, J. M. Ma, W. X. Cao, *Chem. Mater.* **2005**, *17*, 5218–5224; c) H. Li, H. L. Xin, D. A. Muller, L. A. Estroff, *Science* **2009**, *326*, 1244–1247; d) A. Hanisch, P. Yang, A. N. Kulak, L. A. Fielding, F. C. Meldrum, S. P. Armes, *Macromolecules* **2016**, *49*, 192–204.

[3] a) B. Kahr, R. W. Gurney, *Chem. Rev.* **2001**, *101*, 893–951; b) A. G. Shtukenberg, M. D. Ward, B. Kahr, *Chem. Rev.* **2017**, *117*, 14042–14090.

[4] N. Wang, Q. Sun, R. Bai, X. Li, G. Guo, J. Yu, *J. Am. Chem. Soc.* **2016**, *138*, 7484–7487.

[5] G. Lu, S. Li, Z. Guo, O. K. Farha, B. G. Hauser, X. Qi, Y. Wang, X. Wang, S. Han, X. Liu, *Nat. Chem.* **2012**, *4*, 310–316.

[6] a) T. Otto, M. Müller, P. Mundra, V. Lesnyak, H. V. Demir, N. Gaponik, A. Eychmüller, *Nano Lett.* **2012**, *12*, 5348–5354; b) M. Müller, M. Kaiser, G. M. Stachowski, U. Resch-Genger, N. Gaponik, A. Eychmüller, *Chem. Mater.* **2014**, *26*, 3231–3237.

[7] a) A. N. Kulak, P. Yang, Y.-Y. Kim, S. P. Armes, F. C. Meldrum, *Chem. Commun.* **2014**, *50*, 67–69; b) Y. Liu, W. Yuan, Y. Shi, X. Chen, Y. Wang, H. Chen, H. Li, *Angew. Chem. Int. Ed.* **2014**, *53*, 4127–4131; *Angew. Chem.* **2014**, *126*, 4211–4215; c) Y. Liu, H. Zang, L. Wang, W. Fu, W. Yuan, J. Wu, X. Jin, J. Han, C. Wu, Y. Wang, H. L. Xin, H. Chen, H. Li, *Chem. Mater.* **2016**, *28*, 7537–7543.

[8] a) A. E. DiCorato, E. Asenath-Smith, A. N. Kulak, F. C. Meldrum, L. A. Estroff, *Cryst. Growth Des.* **2016**, *16*, 6804–6811; b) E. Asenath-Smith, J. M. Noble, R. Hovden, A. M. Uhl, A. DiCorato, Y.-Y. Kim, A. N. Kulak, F. C. Meldrum, L. F. Kourkoutis, L. A. Estroff, *Chem. Mater.* **2017**, *29*, 555–563.

[9] a) R. Muñoz-Espí, Y. Qi, I. Lieberwirth, C. M. Gómez, G. Wegner, *Chem. Eur. J.* **2006**, *12*, 118–129; b) Y.-Y. Kim, K. Ganesan, P. Yang, A. N. Kulak, S. Borukhin, S. Pechook, L. Ribeiro, R. Kroeger, S. J. Eichhorn, S. P. Armes, B. Pokroy, F. C. Meldrum, *Nat. Mater.* **2011**, *10*, 890–896; c) K. Rae Cho, Y.-Y. Kim, P. Yang, W. Cai, H. Pan, A. N. Kulak, J. L. Lau, P. Kulshreshtha, S. P. Armes, F. C. Meldrum, J. J. De Yoreo, *Nat. Commun.* **2016**, *7*, 10187; d) Y. Ning, L. A. Fielding, K. E. B. Doncom, N. J. W. Penfold, A. N. Kulak, H. Matsuoka, S. P. Armes, *ACS Macro Lett.* **2016**, *5*, 311–315; e) Y. Ning, D. J. Whitaker, C. J. Mable, M. J. Derry, N. J. W. Penfold, A. N. Kulak, D. C. Green, F. C. Meldrum, S. P. Armes, *Chem. Sci.* **2018**, *9*, 8396–8401; f) C. T. Hendley, L. A. Fielding, E. R. Jones, A. J. Ryan, S. P. Armes, L. A. Estroff, *J. Am. Chem. Soc.* **2018**, *140*, 7936–7945; g) Y. Ning, L. Han, M. J. Derry, F. C. Meldrum, S. P. Armes, *J. Am. Chem. Soc.* **2019**, *141*, 2557–2567; h) Y. Ning, L. Han, M. Douverne, N. J. W. Penfold, M. J. Derry, F. C. Meldrum, S. P. Armes, *J. Am. Chem. Soc.* **2019**, *141*, 2481–2489.

[10] a) A. N. Kulak, M. Semsarilar, Y.-Y. Kim, J. Ihli, L. A. Fielding, O. Cespedes, S. P. Armes, F. C. Meldrum, *Chem. Sci.* **2014**, *5*, 738–743; b) A. N. Kulak, R. Grimes, Y.-Y. Kim, M. Semsarilar, C. Anduix-Canto, O. Cespedes, S. P. Armes, F. C. Meldrum, *Chem. Mater.* **2016**, *28*, 7528–7536.

[11] a) Y. Ning, L. A. Fielding, T. S. Andrews, D. J. Growney, S. P. Armes, *Nanoscale* **2015**, *7*, 6691–6702; b) Y. Ning, L. A. Fielding, L. P. D. Ratcliffe, Y.-W. Wang, F. C. Meldrum, S. P. Armes, *J. Am. Chem. Soc.* **2016**, *138*, 11734–11742.

[12] a) W. He, H.-K. Kim, W. G. Wamer, D. Melka, J. H. Callahan, J.-J. Yin, *J. Am. Chem. Soc.* **2014**, *136*, 750–757; b) X. Liu, M.-H. Liu, Y.-C. Luo, C.-Y. Mou, S. D. Lin, H. Cheng, J.-M. Chen, J.-F. Lee, T.-S. Lin, *J. Am. Chem. Soc.* **2012**, *134*, 10251–10258; c) M.

Murdoch, G. I. N. Waterhouse, M. A. Nadeem, J. B. Metson, M. A. Keane, R. F. Howe, J. Llorca, H. Idriss, *Nat. Chem.* **2011**, *3*, 489 – 492; d) J. Lee, H. S. Shim, M. Lee, J. K. Song, D. Lee, *J. Phys. Chem. Lett.* **2011**, *2*, 2840 – 2845; e) R. Jiang, B. Li, C. Fang, J. Wang, *Adv. Mater.* **2014**, *26*, 5274 – 5309; f) S. T. Kochuveedu, J. H. Oh, Y. R. Do, D. H. Kim, *Chem. Eur. J.* **2012**, *18*, 7467 – 7472; g) Y. H. Jang, S. Y. Yang, Y. J. Jang, C. Park, J. K. Kim, D. H. Kim, *Chem. Eur. J.* **2011**, *17*, 2068 – 2076.

[13] Z. L. Wang, *J. Phys. Condens. Matter* **2004**, *16*, R829.

[14] M. Liang, I. C. Lin, M. R. Whittaker, R. F. Minchin, M. J. Monteiro, I. Toth, *ACS Nano* **2010**, *4*, 403 – 413.

[15] Y. Peng, A.-W. Xu, B. Deng, M. Antonietti, H. Cölfen, *J. Phys. Chem. B* **2006**, *110*, 2988 – 2993.

[16] a) S. P. Kawatkar, D. A. Kuntz, R. J. Woods, D. R. Rose, G.-J. Boons, *J. Am. Chem. Soc.* **2006**, *128*, 8310 – 8319; b) B. Gyurcsik, L. Nagy, *Coord. Chem. Rev.* **2000**, *203*, 81 – 149; c) T. Ghoshal, S. Kar, S. Chaudhuri, *Cryst. Growth Des.* **2007**, *7*, 136 – 141.

[17] G. Socrates, *Infrared and Raman characteristic group frequencies: tables and charts*, Wiley, Hoboken, **2004**.

[18] N. J. Richards, D. G. Williams, *Carbohydr. Res.* **1970**, *12*, 409 – 420.

[19] a) S. T. Kochuveedu, Y. H. Jang, D. H. Kim, *Chem. Soc. Rev.* **2013**, *42*, 8467 – 8493; b) J. Xue, O. A. Elbanna, S. Kim, M. Fujitsuka, T. Majima, *Chem. Commun.* **2018**, *54*, 6052 – 6055.

Manuscript received: December 21, 2018
Accepted manuscript online: January 23, 2019
Version of record online: February 20, 2019

